

# BROADBAND FINITE DIFFERENCE TIME DOMAIN MODELING

*Jeffrey J. Daniels<sup>1</sup>, Robert Lee<sup>2</sup>, Yuchan Yi<sup>1</sup>, Ruben Ortega<sup>2</sup>, and Kyle Shalek<sup>1</sup>*

*<sup>1</sup> The Ohio State University, School of Earth Sciences; <sup>2</sup> The Ohio State University, Department of Electrical and Computer Engineering*

## Abstract

Code was designed at The Ohio State University Department of Electrical and Computer Engineering in conjunction with the School of Earth Sciences with the goal of forward modeling subsurface geological systems. To attain this goal the finite difference time domain (FDTD) method was implemented through single- and multi-processor systems leading to the name parallel finite difference time domain (PFDTD). Due to known past problems with the FDTD method our PFDTD code was rigorously tested to define the limits of the parameters in modeling a heterogeneous geological setting. A large frequency range was attained along with a variety of conductivities and permittivities. With these developments and the ability to vary grid cell size the OSU code is able to successfully and accurately forward model realistic complex geological systems.

Most modeling systems have been restricted to modeling in the high frequency regime (>10 MHz), or low frequency region (kilohertz range) to model either displacement currents, or induction, respectively. Our code enables us to generate accurate three dimensional models in the 500 kHz – 10 MHz range, in addition to the higher frequencies. Inputs to the model include variations in conductivity and permittivity over a three dimensional model space. Model results show that reflection images can be generated even at these low frequencies.

## Introduction

Modeling the subsurface of the Earth using Ground Penetrating Radar (GPR) is fraught with complications. The modeling goal is to attain a technique that accurately represents the complexity of nonlinear and heterogeneous subsurface environments using GPR, a noninvasive geophysical method that utilizes electromagnetic waves to image the subsurface. The goal of our research is to produce accurate 3-dimensional forward models of GPR antennas and their interaction with the subsurface. The finite difference time domain (FDTD) method, an electromagnetic modeling technique, was chosen as the best approach for reasons including broadband frequencies, parallel processing, perfectly matched layer (PML) capabilities, and sub-gridding.

This paper explains the current status of our FDTD implementation. Improving on past techniques, the code can be utilized on single- and multiple processor systems which led to the name parallel finite difference time domain (PFDTD). The parallel processing implemented by the MPI (Message Passing Interface) software library greatly improves our computation time for each model run. Along with parallel processing, the code utilizes a PML shell that terminates the model grid boundary. The PML computations provide an accurate representation of the subsurface by accounting for the truncated boundaries of the model and decreasing detrimental edge effects. A current goal is to implement sub-gridding into the model. Sub-gridding certain parts of the model allows increased detail for modeling antenna designs and subsurface targets without the computationally intense approach of

fine-gridding the entire model. Another improvement is increasing the broadband of frequencies which enables us to define the limits of our modeled antennas.

Utilizing these techniques in our model runs shows promising advancements. The PFDTD code is presently able to model antennas with input pulses from 500 kHz to 1GHz. Other input parameters include a wide range of conductivity (0.001-10) and permittivity (1-80). The models have also been tested with the introduction of random stochastic heterogeneity background noise to represent realistic subsurface environments.

## Background Theory

### FDTD

The finite difference time domain (FDTD) method is a robust computational technique useful for modeling electromagnetic processes. It has been used in induction electromagnetic (EM) (Hohmann, 1988; Wang and Hohmann, 1993) and in GPR (Roberts, 1994; Bergmann et al., 1999) studies. Both EM and GPR follow a method first described by Yee (1966). Yee's method uses a staggered-grid approximation of Maxwell's curl relations (Holt, 2004):

$$\nabla \times \mathbf{E} = -\mu \frac{\partial \mathbf{H}}{\partial t} \quad (1)$$

$$\nabla \times \mathbf{H} = \mathbf{j} + \frac{\varepsilon \partial \mathbf{E}}{\partial t} \quad (2)$$

where:

$\varepsilon$  = dielectric permittivity (F/m);  
 $\mu$  = magnetic permeability (H/m);  
 $\mathbf{E}$  = electric field intensity (V/m);  
 $\mathbf{H}$  = magnetic field intensity (A/m);  
 $\mathbf{j}$  = current density (a/m<sup>2</sup>); and  
 $t$  = time (s);

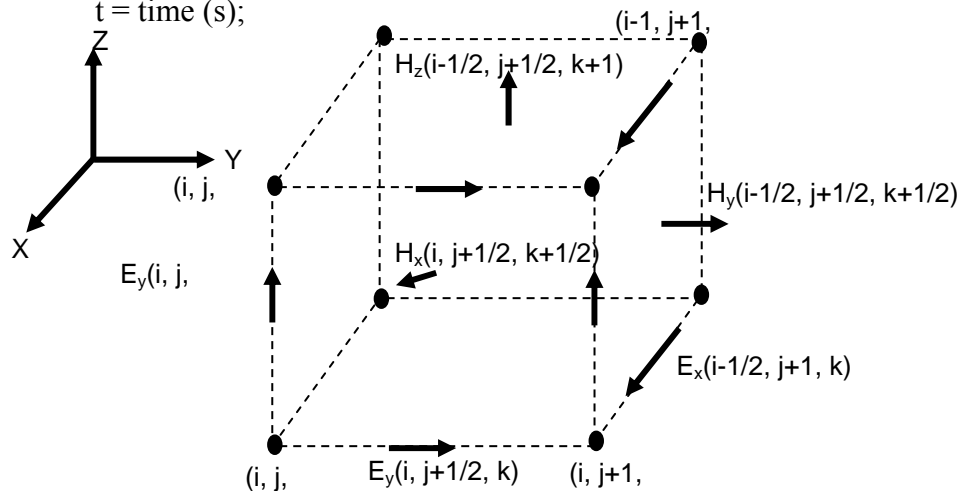


**Figure 1:** Staggered-grid where electric and magnetic field vectors are located tangent to the edges and normal to the sides, respectively (modified from Yee, 1966; Holt, 2004).

The staggered grid (Figure 1) is represented by a perfect square. The electric field ( $\mathbf{E}$ ) values are obtained from the center point of each of the 12 edges. Similarly, a sample is taken from the center of each of the 6 faces, providing the magnetic field ( $\mathbf{H}$ ) values. The electric and magnetic field vectors are

offset in time by one-half of a time step, therefore updating either the electric or magnetic fields requires only previously calculated values (Holt, 2004; Eyuboglu, 2005).

Faraday's Law and Ampere's Law, shown in Equations 1 and 2, can be written in rectangular coordinates as follows (Holt, 2004):

$$\varepsilon \frac{\partial}{\partial t} E_x = \frac{\partial}{\partial y} H_z - \frac{\partial}{\partial z} H_y - \sigma E_x \quad (3) \quad \varepsilon \frac{\partial}{\partial t} E_y$$

$$= \frac{\partial}{\partial z} H_x - \frac{\partial}{\partial x} H_z - \sigma E_y \quad (4)$$

$$\varepsilon \frac{\partial}{\partial t} E_z = \frac{\partial}{\partial x} H_y - \frac{\partial}{\partial y} H_x - \sigma E_z \quad (5)$$

$$\mu \frac{\partial}{\partial t} H_x = \frac{\partial}{\partial z} E_y - \frac{\partial}{\partial y} E_z \quad (6)$$

$$\mu \frac{\partial}{\partial t} H_y = \frac{\partial}{\partial x} E_z - \frac{\partial}{\partial z} E_x \quad (7)$$

$$\mu \frac{\partial}{\partial t} H_z = \frac{\partial}{\partial y} E_x - \frac{\partial}{\partial x} E_y \quad (8)$$

where  $\sigma$  = conductivity at a specific point in the grid (S/m).

The central difference approximation can be calculated as follows:

$$\frac{\partial}{\partial \xi} f(\xi) \approx \frac{f(\xi + \Delta\xi/2) - f(\xi - \Delta\xi/2)}{\Delta\xi} \quad (9)$$

$$f(i\Delta x, j\Delta y, k\Delta z, n\Delta t) = f^n(i, j, k). \quad (10)$$

Equations 9 and 10 yield the finite difference approximations of  $E_x$  at the location  $(i+1/2, j, k)$  and time step  $(n+1)$  and  $H_y$  at the location  $(i+1/2, j, k+1/2)$  and time step  $(n+1/2)$  (Roberts, 1994), as seen below:

$$E_x^{n+1} \left( i + \frac{1}{2}, j, k \right) = \frac{2\varepsilon \left( i + \frac{1}{2}, j, k \right) - \sigma \left( i + \frac{1}{2}, j, k \right) \Delta t}{2\varepsilon \left( i + \frac{1}{2}, j, k \right) + \sigma \left( i + \frac{1}{2}, j, k \right) \Delta t} E_x^n \left( i + \frac{1}{2}, j, k \right) \quad (11)$$

$$+ \frac{2\Delta t}{2\varepsilon \left( i + \frac{1}{2}, j, k \right) + \sigma \left( i + \frac{1}{2}, j, k \right) \Delta t} \left[ \frac{H_x^{n+1/2} \left( i + \frac{1}{2}, j + \frac{1}{2}, k \right) - H_x^{n+1/2} \left( i + \frac{1}{2}, j - \frac{1}{2}, k \right)}{\Delta y} - \frac{H_y^{n+1/2} \left( i + \frac{1}{2}, j, k + \frac{1}{2} \right) - H_y^{n+1/2} \left( i + \frac{1}{2}, j, k - \frac{1}{2} \right)}{\Delta z} \right]$$

$$H_y^{n+1/2} \left( i + \frac{1}{2}, j, k + \frac{1}{2} \right) = H_y^{n-1/2} \left( i + \frac{1}{2}, j, k + \frac{1}{2} \right) - \quad (12)$$

$$\frac{\Delta t}{\mu \left( i + \frac{1}{2}, j, k + \frac{1}{2} \right)} \left[ \frac{E_x^n \left( i + \frac{1}{2}, j, k + 1 \right) - E_x^n \left( i + \frac{1}{2}, j, k + 1/2 \right)}{\Delta x} - \frac{E \left( i + \frac{1}{2}, j, k + 1 \right) - E \left( i + \frac{1}{2}, j, k \right)}{\Delta z} \right]$$

The other components of the  $\mathbf{E}$  and  $\mathbf{H}$  fields are found in the same way as described above.

## PML

The perfectly matched layer PML is a non-physical material boundary neighboring the computational domain (Gurel and Oguz, 2000). After the original work by Berenger (1994), the theory of PML for reflectionless absorption of electromagnetic fields and its implementation has become a popular research area (Chew and Weedon, 1994; Katz et al., 1994; Reuter et al., 1994; and Bahr et al., 1995). Sacks et al. (1995) studied the PML formulation based on lossy anisotropic media. Their PML formulation is based on Maxwell's equations without modifications unlike Berenger's. Sacks et al. (1995) applied this PML formulation to the finite element method in the frequency domain. Gedney (1996) showed that a lossy uniaxial medium can be perfectly matched to an isotropic space by properly choosing the constitutive parameters of the medium. Gedney's PML formulation can be applied to the FDTD methods based on generalized grids or the finite element methods. Its application to the FDTD method is more computationally efficient than Berenger's PML method (Gedney, 1996).

Rao et al. (2001) pointed out the importance of deriving a PML formulation that can terminate lossy media in their study. This isotropic medium is characterized by:

$$\begin{aligned} \nabla * \mathbf{E} &= -j\omega\mu[\Lambda]\mathbf{H} \\ \nabla * \mathbf{H} &= j\omega\varepsilon_{eff}[\Lambda]\mathbf{E} \end{aligned}$$

where

$$[\Lambda] = \begin{pmatrix} \frac{s_y s_z}{s_x} & 0 & 0 \\ 0 & \frac{s_x s_z}{s_y} & 0 \\ 0 & 0 & \frac{s_y s_x}{s_z} \end{pmatrix}, \quad s_p = 1 + \frac{\sigma_p}{j\omega} \quad (13)$$

A careful choice of material properties for all polarizations, frequencies and angles of incidence can provide a reflectionless interface. However, permittivity takes the form  $\varepsilon_{eff} = \varepsilon + \frac{\sigma}{j\omega}$  for lossy media and therefore the original formulation needs to be modified (Rao et al., 2001). The second curl equation is given by:

$$\left(1 + \frac{\sigma_p}{j\omega}\right) (\nabla_x \vec{H})_p = j\omega \left(\varepsilon + \frac{\sigma}{j\omega}\right) \left(1 + \frac{\sigma_q}{j\omega}\right) \left(1 + \frac{\sigma_r}{j\omega}\right) E_p \quad (14)$$

In this equation, p, q, and r represent the coordinate directions. This equation also has  $\frac{1}{(j\omega)^2}$  dependence and we solve it by introducing a scaled electric field  $\vec{D}$  (Rao et al., 2001).

$$\left(1 + \frac{\sigma_p}{j\omega}\right) (\nabla_x \vec{H})_p = j\omega \left(1 + \frac{\sigma_q}{j\omega}\right) \left(1 + \frac{\sigma_r}{j\omega}\right) D_p \quad (15)$$

Where

$$D_p = \left(\varepsilon + \frac{\sigma}{j\omega}\right) E_p \quad (16)$$

Then, by discretizing these equations:

$$\begin{aligned}
D_p^{n+1} &= \left[ \frac{2 - (\sigma_q + \sigma_r)\Delta t}{2 + (\sigma_q + \sigma_r)\Delta t} \right] D_p^n - \left[ \frac{2\sigma_q\sigma_r(\Delta t)^2}{2 + (\sigma_q + \sigma_r)\Delta t} \right] \sum_{m=0}^n D_p^m + \left[ \frac{(2 + \sigma_p\Delta t)\Delta t}{2 + (\sigma_q + \sigma_r)\Delta t} \right] (\nabla_x \bar{H})_p^{n+\frac{1}{2}} \\
&+ \left[ \frac{2\sigma_q(\Delta t)^2}{2 + (\sigma_q + \sigma_r)\Delta t} \right] \sum_{m=0}^{n-1} (\nabla_x \bar{H})_p^{m+\frac{1}{2}} \\
E_p^{n+1} &= \frac{2}{2\varepsilon + \sigma\Delta t} \left( D_p^{n+1} - \sigma\Delta t \sum_{m=0}^n E_p^m \right) \tag{17}
\end{aligned}$$

The electric field can be updated by using this equation. The updated equation for magnetic field is:

$$\begin{aligned}
H_p^{n+1} &= \left[ \frac{2 - (\sigma_q + \sigma_r)\Delta t}{2 + (\sigma_q + \sigma_r)\Delta t} \right] H_p^n - \left[ \frac{2\sigma_q\sigma_r(\Delta t)^2}{2 + (\sigma_q + \sigma_r)\Delta t} \right] \sum_{m=0}^n H_p^m - \left[ \frac{(2 + \sigma_p\Delta t)\Delta t}{2 + (\sigma_q + \sigma_r)\Delta t} \right] (\nabla_x \bar{E})_p^{n+\frac{1}{2}} - \\
&\left[ \frac{2\sigma_q(\Delta t)^2}{2 + (\sigma_q + \sigma_r)\Delta t} \right] \sum_{m=0}^{n-1} (\nabla_x \bar{E})_p^{m+\frac{1}{2}} \tag{18}
\end{aligned}$$

These basic equations have been programmed and are fully operational for 3D modeling of any subsurface configuration of geology or objects emplaced below the surface. The model accommodates antenna positions above, or below the ground surface. The model is robust enough to handle any subsurface or surface objects, including above-ground obstructions.

## Numerical Computations and Implementation

The FDTD modeling code used in this research was created by the Electro Science Laboratory at The Ohio State University (Rao et al., 2001). The modeling program was developed using the C++ programming language. An anisotropic PML was used to prevent reflections from the truncated boundary. The conductivity of the PML is chosen to establish a quadratic profile in the outward direction along which the attenuation is preferred (Rao et al., 2001). The PML layers are 20 cells thick on all sides. The permittivity and conductivity of the PML layer are matched to the adjacent Maxwell region for impedance continuity.

The incident wave of FDTD modeling for PML test case was excited by a second derivative of the Gaussian pulse as an infinitesimal dipole in the Maxwell region;

$$J_y(t) = 2(2X^2 - 1) \exp(-X^2) / T_b \tag{19}$$

where

$$X = (t - t_0) / T_b \tag{20}$$

$$T_0 = 3.2T_b \tag{21}$$

$$T_b = \sqrt{\frac{2 \log\left(\frac{f_{\max}}{f_{\min}}\right)}{\pi(f_{\max}^2 - f_{\min}^2)}} \tag{22}$$

The model grids in the PFDTD program consist of the Maxwell domain and the PML shell surrounding the former. At the setup step of the modeling program, all the grid cells are initialized with data of the constitutive parameters input to the program. The next one is the core step of numerical computation: the time loop of solving the Maxwell's curl equations. At time step  $n$  in the loop, all the  $\mathbf{E}$  field 3D vectors are updated, that is, spatially integrated over the entire Maxwell domain and the PML blocks corresponding to equation (1). Then the  $\mathbf{E}$  field values at voltage source locations are added. At the time step  $(n+1/2)$ , all the  $\mathbf{H}$  field vectors are updated corresponding to equation (2). At the end of

each time step, any components of the  $\mathbf{E}$  and  $\mathbf{H}$  field vectors are output or monitored at any grid cells including that of the receiver antenna.

## Output Examples

### *FDTD Antenna Simulation*

Antennas usually perform well only over a relatively narrow bandwidth. For simple dipole-type antennas, the input impedance of the antenna can vary rapidly with frequency due to the reflections from the ends of the dipole. In an effort to reduce reflections on an antenna structure, resistive loading was applied at the ends of a V-dipole antenna model. The resistive loading was modeled as a 1 FDTD Yee cell thick block with a conductivity corresponding to a desired resistance according to  $R = 1/\sigma\tau$ , where  $R$  is the desired resistance,  $\sigma$  is the cell conductivity and  $\tau$  is the cell thickness. The resistively loaded section modeled had a linear resistance profile varying from  $30\Omega$  to  $300\Omega$ . The antenna was excited with a differential Gaussian pulse with a center frequency of 450 MHz. Two configurations were simulated as shown below.

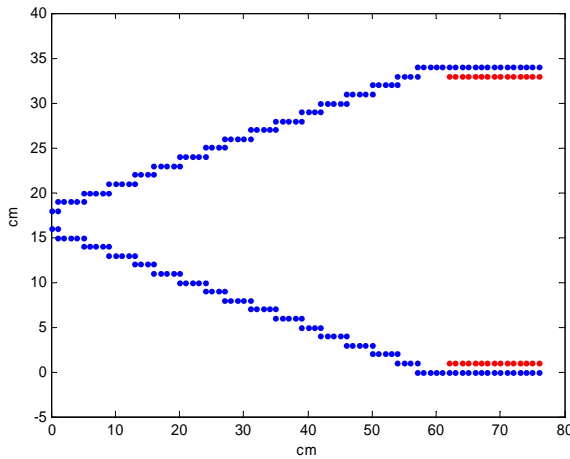


**Figure 2:** Layered Configuration.

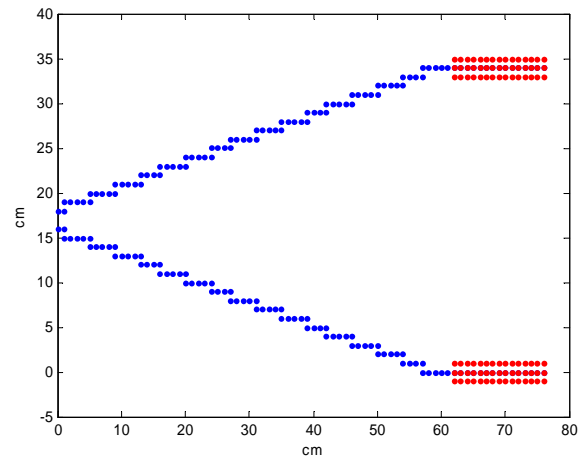


**Figure 3:** Wrapped Configuration.

Above, the blue points represent perfect electric conducting (PEC) FDTD Yee cells, used to model an ideal antenna structure. The red points represent dielectric FDTD Yee cells, used to model the resistively loaded section of the antenna structure. The “layered” configuration was modeled as the resistively loaded section consisting of a single layer coating to the “inside” of the antenna arms. The “wrapped” configuration was modeled as the resistively loaded section consisting of a single layer coating around the circumference of the end of the two antenna arms. The idea is that use of the resistive card structure will attenuate the current flowing on the antenna structure and thus, reduce reflection once the current reaches the end of the antenna arm.

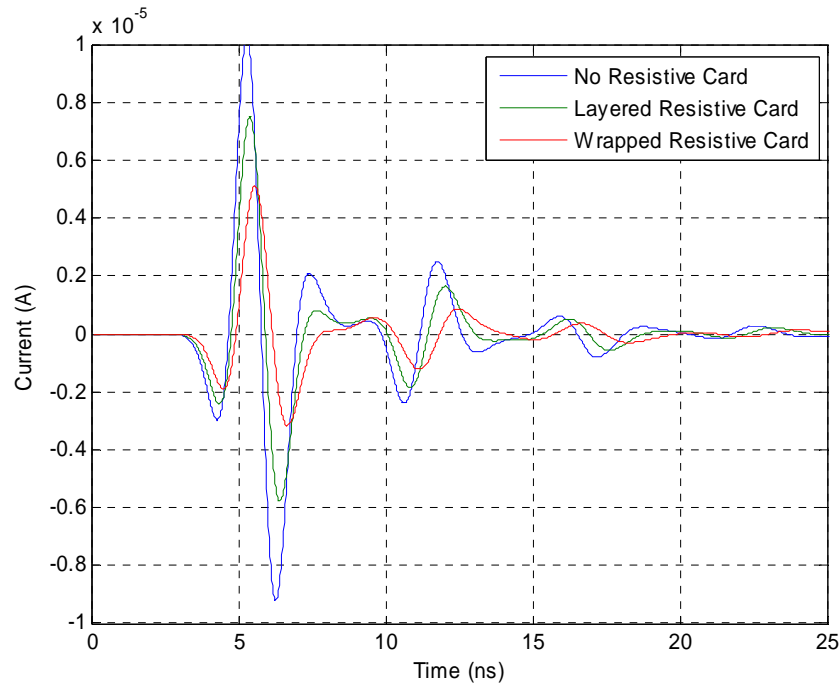


**Figure 4:** Current on V-dipole antenna

In Figure 4, above, numerical results from the FDTD simulation were taken, and the current on the top arm of the antenna structure was determined at a position 8cm from the end of the antenna (approximately half way “into” the resistively loaded section). The results show that application of the resistive material on the antenna does in fact attenuate the flow of current in the antenna, resulting in less antenna ringing. The wrapped configuration seems to perform better than the layered configuration.

#### *Two dimensional void filled with air or water*

Figure 5 shows the anomaly of  $E_y$  field along a 28 meter line of 40 traces computed for the FDTD models of 0.31 million cubic cells of a linear size 0.67 m. The anomaly was caused by reflections from a 2 x 2 m void lying 20 m below the surface in the y-direction perpendicular to the line of observation (in the x-direction). The center frequency of the GPR pulse is 10 MHz. The mean value of the background dielectric constant is 5 and that of conductivity is 0.005. The standard deviation of the background dielectric constant is 1 for the randomly heterogeneous model.

#### *3D pseudo images*

On the left side, Figure 6 shows another FDTD model with a 2 x 2 m void at 20 m below the surface. The FDTD model consists of 0.62 million cubic cells of a linear size 0.67 m. Right two images in the Figure are 3D pseudo images that were made of anomaly traces along 9 lines on the surface. Each line of 60 traces is 83 m long. The center frequency is 10 MHz, the background dielectric constant is 5, and the background conductivity is 0.005.

## Conclusions

The PFDTD code was rigorously tested to define the limits of the parameters in modeling a heterogeneous geological setting. A frequency range of 500 kHz to 2GHz was attained along with a variety of conductivities and permittivities. With these developments and the ability to vary grid cell

size the OSU code is able to successfully and accurately forward model realistic complex geological systems.

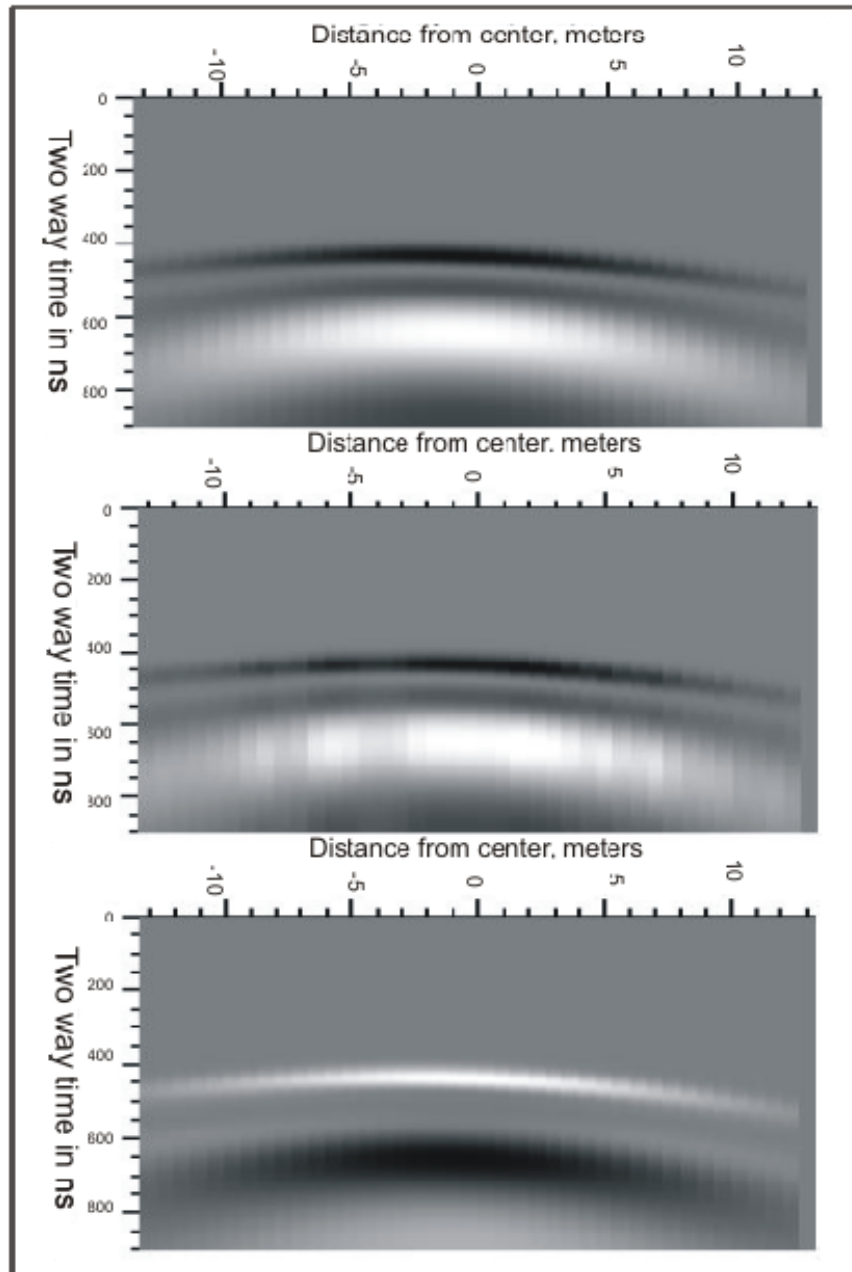


**Figure 5:** Ey anomaly for background means  $\epsilon_r=5$  and  $\sigma=0.005$  (upper: homogeneous background/air-filled void; middle: heterogeneous/air-filled; lower: homogeneous/water-filled).

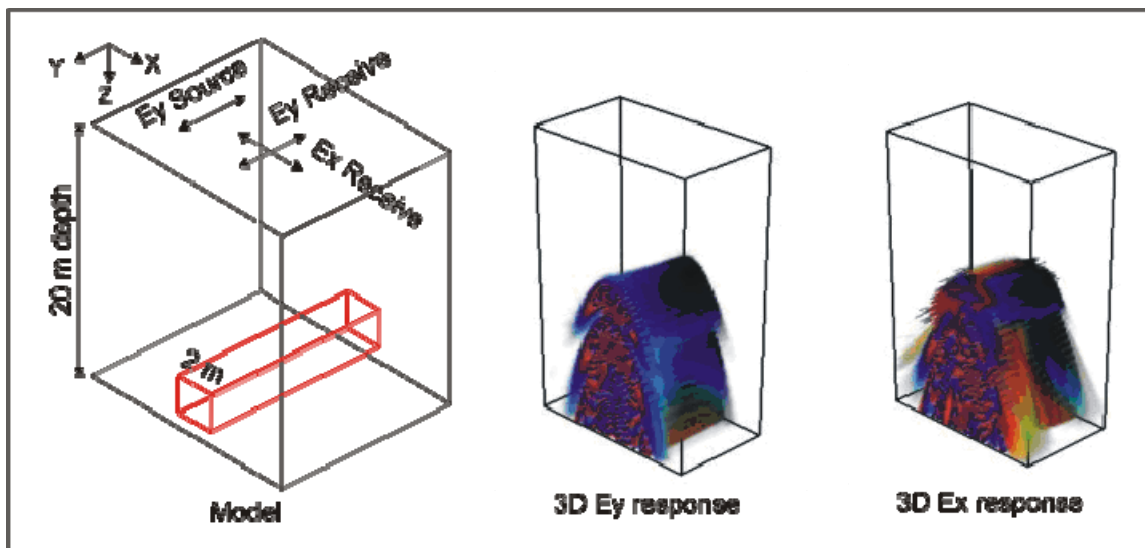


**Figure 6:** 3D displays for model results from a 2x 2 m void buried at a depth of 20 m. The 3D plot is generated by anomalies along 9 lines each of which is made of 60 traces. The two components (Ex and Ey) represent measurements in orthogonal directions at each point.

## References

- Bahr, A., Lauer, A., and Wolff, I., 1995, Application of the PML absorbing boundary condition to the FDTD analysis of microwave circuits, *IEEE MTT-S Int. Microwave Symp. Dig.*, pp. 27-30.
- Berenger, J.P., 1994, A perfectly matched layer for the absorption of electromagnetic waves, *Journal of Computational Physics*, vol. 114, pp. 185-200.
- Bergmann, T., J. O. Blanch, J. O. A. Robertsons, K. Holliger, 1999, A Simplified Lax-Wendroff Correction for Staggered-grid FDTD Modeling of Electromagnetic Wave Propagation in Frequency-Dependent Media, *Geophysics*, 64, no. 5, pg. 1369-1377.
- Chew, W.C., and Weedon, W.H., 1994, A 3-D perfectly matched medium from modified Maxwell's equations with stretched coordinates, *Microwave Opt. Technol. Lett.*, pp. 599-604, September.
- Daniels, J.J., Roberts, R., Schilling, B., and Erickson, R., 1992, "GPR measurements for locating underground mine workings at an active open-pit mine": *Trans. Of the Fourth International Conference on Ground Penetrating Radar*, June 8-13, 1992, Rovaniemi, Finland.
- Daniels, J.J., Grumman, D., and Vendl, M., 1997, Coincident antenna Three Dimensional GPR: *Jour. Env. Eng. Geoph.*, V. 2, No. 1, p. 1-9.
- Eyuboglu, S., 2005, Applications of ground penetrating radar for environmental and geotechnical problems, *PhD Dissertation*, Department of Applied Sciences, University of Arkansas at Little Rock.
- Gedney, S.D., 1996, An anisotropic perfectly matched layer – absorbing medium for the truncation of FDTD lattices, *IEEE Trans. Ant. Prop.*, vol. 44, no. 12.
- Gurel, L., and Oguz, U., 2000, Three-dimensional FDTD modeling of a ground-penetrating radar, *IEEE Transactions on Geoscience and Remote Sensing*, vol. 38, no. 4, pp. 1513-1521.
- Holt, J. J., 2004, Finite difference time domain modeling of dispersion from heterogeneous ground properties in ground penetrating radar, *PhD Thesis*, Department of Geological Sciences, The Ohio State University.

- Katz, D.S., Thiele, E.T., and Taflove, A., Validation and extension to three dimensions of the Berenger PML absorbing boundary condition for FDTD meshes, *IEEE Microwave Guided Wave Letter*, vol. 4, pp.268-270.
- Pyke, K., Daniels, J. J., Vendl, M., and Eyuboglu, S., 2006, Controlled Experiment to Determine GPR Water Table Response and FDTD modeling. In Review, *Journal of Environmental and Engineering Geophysics*.
- Rao, R K., Lee, K-H., Chen, C-C., and Lee, R., 2001, Application of full-polarimetric ground penetrating radar for buried UXO classification, Lecture notes, ElectroScience Laboratory, Department of Electrical Engineering, The Ohio State University.
- Reuter, C.E., Joseph, R.M, Thiele, E.T., Katz, D.S., and Taflove, A., 1994, Ultrawideband absorbing boundary condition for termination of waveguiding structures in FDTD simulations, *IEEE Microwave Guided Wave Letter*, vol. 4, pp.344-346, October.
- Roberts, R.L., and Daniels, J.J., and Peters, L., 1992, Improved GPR interpretation from analysis of buried target polarization properties: *Proceedings of SAGEEP*, April 26-29, 1992, Oakbrook, IL, p.597-611.
- Roberts, R.L., and Daniels, J.J., 1993, Analysis of the effectiveness of velocity-depth inversion using bistatic data collected over targets of different sizes, shapes, and orientations: *Proceedings on Advanced Ground Penetrating Radar, Second Govt. Workshop on GPR*, The Ohio State University Columbus, OH, Oct.26-28, 1993.
- Roberts, R. L., 1994, Analysis and Theoretical Modeling of GPR Polarization Data, PhD Thesis, The Ohio State University.
- Roberts, R.L., and Daniels, J.J., 1997, Modeling Near Field GPR in three dimensions using the FDTD Method: *Geophysics*, Vol. 62, No. 4, p. 1114-1126.
- Sacks, Z. S., Kingsland, D. M., Lee, R., and Lee, J. F., 1995, A perfectly matched anisotropic absorber for use as an absorbing boundary condition, *IEEE Transactions on Antennas and Propagation*, vol. 43, pp. 1460-1463.
- Wang, T., and Hohmann, G. W., 1993, A finite difference time domain solution for three dimensional electromagnetic modeling, *Geophysics*, Vol. 58, pp. 797-809.
- Wang, G.L., Chew, W.C., Cui, T.J., Aydiner, A.A., Wright, D.L., and Smith, D.V., 2004, 3D near-to-surface conductivity reconstruction by inversion of VETEM data using the distorted Born iterative method: *Inverse Problems*, (Special Section on Electromagnetic Characterization of Buried Obstacles) Vol 20, No. 6, p. S195- S216.
- Yee, K. S., 1966, Numerical Solutions of Initial Boundary Value Problems Involving Maxwell's Equation in Isotropic Material, *IEEE Trans. Anten. Propa.*, vol. AP-14, no. 3, pg. 302-307.